This is a preprint, the final version is subject to change, of the American Mineralogist (MSA)
Cite as Authors (Year) Title. American Mineralogist, in press.
DOI: https://doi.org/10.2138/am-2019-6658

# Revision 3

## Compressibility of two Na-rich clinopyroxenes: A synchrotron single-crystal X-ray diffraction study

EKATERINA A. MATROSOVA[1,*], LEYLA ISMAILOVA[2], ANDREY V. BOBROV[1,3,4], ELENA BYKOVA[5], MAXIM BYKOV[6], KONSTANTIN GLAZYRIN[5], LUCA BINDI[7,8], SERGEY V. OVSYANNIKOV[6], SERGEY M. AKSENOV[9,10], DMITRY YU. PUSHCHAROVSKY[3], LEONID DUBROVINSKY[6]

[1] Vernadsky Institute of Geochemistry and Analytical Chemistry of Russian Academy of Sciences, Moscow, Russia 119991
[2] Skolkovo Institute of Science and Technology, Skolkovo Innovation Center, 3, Moscow, Russia 143026
[3] Geological Faculty, Moscow State University, Moscow, Russia 119991
[4] Institute of Experimental Mineralogy of Russian Academy of Sciences, Chernogolovka, Russia 142432
[5] Photon Sciences, Deutsches Elektronen-Synchrotron, Notkestrasse 85, D-22607 Hamburg, Germany
[6] Bayerisches Geoinstitut, University of Bayreuth, Universitätsstrasse 30, D-95440 Bayreuth, Germany
[7] Dipartimento di Scienze della Terra, Università di Firenze, Via La Pira 4, 50121 Florence, Italy
[8] CNR - Istituto di Geoscienze e Georisorse, sezione di Firenze, Via La Pira 4, 50121 Florence, Italy
[9] FSRC "Crystallography and Photonics", Russian Academy of Sciences, Moscow, Russia 119333
[10] Nesmeyanov Institute of Organoelement Compounds, Russian Academy of Sciences, Moscow, Russia, 119334

*Corresponding Author: ekaterina.a.sirotkina@gmail.com

## Abstract

Synchrotron-based high-pressure single-crystal X-ray diffraction experiments were conducted on synthetic clinopyroxenes at room temperature to a maximum pressure of 40 GPa. We studied two crystals with different composition. A Na-Ti-pyroxene with formula $(Na_{0.86}Mg_{0.14})(Mg_{0.57}Ti_{0.43})Si_2O_6$ synthesized at $P$ = 7 GPa and $T$ = 1700 °C, and a Na-pyroxene with composition $(Na_{0.886}Mg_{0.085}Fe_{0.029})(Si_{0.442}Mg_{0.390}Fe_{0.168})Si_2O_6$ synthesized at $P$ = 15 GPa and $T$ = 1500 °C. These phases were found to be monoclinic with the space group $C2/c$ and exhibit $K_{To}$ of 106.8(2), 121.8(4) GPa, respectively. Na-Ti-pyroxene is more compressible than Fe-bearing Na-Mg-Si-pyroxene, likely due to the fact that the $FeO_6$ octahedron is significantly more rigid than $MgO_6$ at high pressure. The formation of Na-rich pyroxenes in the deep mantle is related to crystallization of low-degree alkaline carbonate-silicate melts formed when the crust and mantle interact during the slab descent and its stagnation in the transition zone.

**Keywords:** pyroxene, single-crystal X-ray diffraction, high-pressure, high-temperature, phase transitions, equation of state, Earth's mantle

## Introduction

It is well known that pyroxenes may undergo a number of phase transitions with increasing *P* and *T* toward at least five different structures (Cameron and Papike 1981; Yang and Prewitt 2000). These transitions typically affect all the physical properties of the mineral including density, bulk modulus, and the orientation and dimensions of the unit-strain ellipsoid. Knowledge of the behavior of mantle materials at high *P* is crucial for understanding of the deep Earth structure and composition. In addition, thermodynamic parameters of pyroxene end-members are critical for thermo- and geodynamic modeling of the Earth's upper mantle (Stixrude and Lithgow-Bertelloni 2005).

The most common pyroxenes are those that contain the major elements (Ca, Mg, and Fe) in the M sites (enstatite, ferrosilite, diopside, hedenbergite). Their early HP-XRD-studies (Hazen and Finger 1977; Levien and Prewitt 1981) formed the basis for such important scientific interdisciplinary problem as comparative crystal chemistry of the mantle and core minerals. The results obtained showed that the three polyhedra (M1, M2 and Si) in pyroxene structures decrease irregularly in size and their compressibilities depend on their chemical contents. Somewhat less common are pyroxenes that incorporate larger cations, such as Na. For this reason, Na-rich pyroxenes have been much less studied.

It has long been assumed that clinopyroxenes abundant in the Earth's crust and upper mantle contain only tetrahedrally coordinated Si. The synthesis of $Na(Mg_{0.5}Si_{0.5})Si_2O_6$ pyroxene and its unit-cell parameters were originally reported based upon X-ray powder (Gasparik 1988) and single-crystal (Angel et al. 1988) diffraction. The compound was found to be monoclinic with space group *P*2/*n*. These studies have shown that clinopyroxenes may accommodate octahedrally-coordinated silicon (Yang and Konzett 2005) suggesting that the stability of clinopyroxenes may be expanded to higher pressures than those previously assumed. Later Yang et al. (2009) synthesized five clinopyroxenes containing various amounts of six-coordinated silicon in the $Na(Mg_{0.5}Si_{0.5})Si_2O_6$–$NaAlSi_2O_6$ system at 15 GPa and 1600°C. These authors showed that clinopyroxenes with $^{VI}Si \leq 0.33$ atoms per formula unit (apfu) possess *C*2/*c* symmetry, whereas those with $^{VI}Si \geq 0.45$ apfu crystallize with *P*2/*n* symmetry. Increasing $^{VI}Si$ content from 0.33 to 0.45 apfu results in the formation of the discontinuity in the unit-cell parameters suggesting that the *C*2/*c*-*P*2/*n* transition is first-order in character (Yang et al. 2009). The *P*–*V*–*T* equation of state (EoS) was studied for Na-pyroxene at pressures up to 21 GPa and temperatures up to 1400°C by *in situ* X-ray diffraction experiments using a Kawai-type multi-anvil apparatus (Dymshits et al. 2015).

Another probable high-pressure Na-pyroxene with $Ti^{4+}$ in the octahedral site is $Na(Mg_{0.5}Ti_{0.5})Si_2O_6$ (Na-Ti-Px). Such Na-Ti-pyroxenes are poorly studied, while the crystal structure of Na-Ti pyroxene with the composition $NaTi^{3+}Si_2O_6$ has been deeply investigated (e.g., Prewitt et al. 1972; Ninomiya et al. 2003; Redhammer et al. 2003). The synthesis of $NaTi^{3+}Si_2O_6$ single crystals and the full description of the room-temperature structure have been first done by Ohashi et al. (1982). At 298 K, the compound has monoclinic symmetry with space group *C*2/*c*. Ohashi (2003) reported the structural

differences in $(Na,Ca)(Ti^{3+},Mg)Si_2O_6$ clinopyroxenes with various compositions at ambient conditions. Recently, Ullrich et al. (2010) investigated the influence of the coupled substitution $Na^{+}Ti^{3+} \leftrightarrow Ca^{2+}Mg^{2+}$ on the structural stability of $NaTi^{3+}Si_2O_6$ at high pressures. These authors showed that, in contrast to the composition $(NaTi^{3+}Si_2O_6)_{0.54}(CaMgSi_2O_6)_{0.46}$, this pyroxene underwent the $C2/c$–$P\bar{1}$ phase transition at a pressure higher than 4.37 GPa.

The synthesis of $(Na_{0.86}Mg_{0.14})(Mg_{0.57}Ti_{0.43})Si_2O_6$ pyroxene with octahedral titanium and its structural details were originally reported by Sirotkina et al. (2016). This study has shown that clinopyroxene may accommodate octahedrally-coordinated $Ti^{4+}$. The isomorphic replacement in this compound with respect to $Mg_2Si_2O_6$ corresponds to the scheme: $Na^{+} + (Ti^{4+})/2 + (Mg^{2+})/2 = 2Mg^{2+}$. The $Na(Mg_{0.5}Ti_{0.5})Si_2O_6$ component has been sometimes registered as an end-member of natural low-Ca mantle pyroxenes (Bishop et al. 1978; Rudnick et al. 2004; Aulbach et al. 2004; Sirotkina et al. 2016).

Na-rich clinopyroxenes have not been deeply studied at high pressures. Zhao et al. (1997) performed a synchrotron X-ray powder diffraction study on jadeite up to 8.2 GPa and 1280 K. They fit their data with a modified Birch-Murnaghan equation of state, with $K'_0 = 5.0$, and found the bulk modulus of jadeite to be 125(4) GPa. Nestola et al. (2006) studied jadeite and aegirine compressibilities, as a function of pressure, and examined changes in compressional anisotropy with variations in chemistry along the jadeite-aegirine ($NaFeSi_2O_6$) solid solution.

To shed light on the high-pressure behavior of Na-rich clinopyroxenes, here we report the single-crystal X-ray diffraction study of two pyroxenes with composition $(Na_{0.86}Mg_{0.14})(Mg_{0.57}Ti_{0.43})Si_2O_6$ and $(Na_{0.884}Fe^{2+}_{0.116})(Mg_{0.475}Si_{0.442}Fe^{2+}_{0.083})Si_2O_6$ up to a pressure of 40 GPa. Furthermore, in an effort to understand the variation in Na-rich

pyroxene compressibilities, a series of Na-clinopyroxenes from the literature is also examined.

## Experimental methods

Synthesis of a new Na-Ti-pyroxene with formula $(Na_{0.86}Mg_{0.14})(Mg_{0.57}Ti_{0.43})Si_2O_6$ was performed at the Vernadsky Institute of Geochemistry and Analytical Chemistry, Russian Academy of Sciences, Moscow, Russia, using the high-pressure toroidal 'anvil-with-hole' apparatus at 7 GPa and 1700 °C. The starting mixture was chemically pure oxides of Mg, $Ti^{4+}$ and Si and sodium silicate $Na_2SiO_3$ corresponding to the formula $Na_2MgTi_2Si_3O_{12}$. Solid-state cells of a 30-mm outer diameter were manufactured from pressed mixture of MgO and BN in equal parts (with a small amount of $Cr_2O_3$). They contained an ultrapure graphite heater with an outer diameter of 7 mm and a length of 7.5 mm, which had a hole with a diameter of 2.5 mm and a depth of 2.5 mm. This hole was the container for starting materials. The temperature measurement accuracy was ±10 °C. Run pressure was controlled to ±0.5 GPa. Details of the experimental techniques and cell calibration were described by Bobrov and Litvin (2009). Colorless transparent crystals of Na-Ti-Px, ~150 μm in size, were observed in the quenched groundmass of elongated rutile and pyroxene crystals in the run carried out at $P$ = 7 GPa and $T$ = 1700 ºC (Fig. 1a).

The Fe-bearing Na-Mg-Si pyroxene with the composition $(Na_{0.886}Mg_{0.085}Fe_{0.029})(Si_{0.442}Mg_{0.390}Fe_{0.168})Si_2O_6$ was synthesized on a 2000-t Kawai-type high-pressure multi-anvil apparatus at the Bayerisches Geoinstitut, Bayreuth, Germany, at 14 GPa and 1500 °C. The details of experimental assembly and procedures were described elsewhere (Frost et al. 2004). The starting material (90 mol % $Na(Mg_{0.5}Si_{0.5})Si_2O_6$ + 10 mol % $Fe_2Si_2O_6$) was prepared from chemically pure oxides

(MgO, FeO, and $SiO_2$) and sodium silicate $Na_2SiO_3$, homogenized at room temperature using ethanol and then dried in the stove at 100 °C. A starting mixture was placed into a capsule of 3.5 mm in height and 2 mm in diameter made of a rhenium foil. The high temperature was generated using a $LaCrO_3$ heater. The capsule was isolated from the heater by a MgO cylinder. The cell assembly with the sample was compressed between eight cubic tungsten carbide anvils with corners truncated to 5.0 mm edge lengths. The accuracy in determination of pressure and temperature was estimated to be ±0.5 GPa and ±50 °C, respectively. The run duration was 2 h. Then, the sample was rapidly quenched to ambient temperature by switching off a power supply with a quench rate of 200 °C/s. Fig. 1b shows the secondary electron image of Na-pyroxene aggregates in a groundmass composed of very small pyroxene and stishovite grains.

After runs, sample with Na-Ti pyroxene was embedded in epoxy and polished to study texture and phase compositions. The compositions of the run products were analyzed by means of a JEOL JSM-6480LV scanning electron microscope equipped with an Oxford X-MaxN energy-dispersive analytical setup at the Department of Petrology, Geological Faculty, Moscow State University. The following standards were used: NaCl for Na, $TiO_2$ for Ti, diopside for Si and Mg, and synthetic $Fe_2SiO_4$ for Fe. Compositions of the phases were determined from the average of 4–6 analyses performed at an accelerating voltage of 20 kV and beam current of 10 nA.

Pre-selected isometric crystals of ~ 15 μm were loaded in diamond anvil cells (DACs) into holes drilled through Re gaskets indented to 20-35 μm thickness. After the study at ambient conditions, DACs were loaded with Ne to achieve quasi-hydrostatic conditions. Neon was also used as a pressure standard using the equation of state (Fei et al. 2007). For pressure measurements below 15 GPa, the fluorescence emission of a ruby

chip was used. Two separate synchrotron-based X-ray diffraction experiments were performed at the ESRF, Grenoble, France, at the beamline ID09A and at the DESY of PETRA III, Hamburg, Germany, at the extreme conditions beamline P02.2. At the ESRF on beamline ID09, we used a mar555 flat panel detector and an X-ray wavelength of 0.415 Å with a beam spot size of ~10 x 10 $\mu m^2$. At the extreme conditions beamline P02.2 at PETRA III, we used X-ray wavelength of 0.2903 Å and a Perkin Almer detector, and the beam-size was 3 x 8 $\mu m^2$. The positions of the detectors were calibrated using Si or $CeO_2$ standards.

Single-crystal diffraction data were collected at various pressures in two modes. Wide scans were collected during ω rotation scans of ±20° with 40 s per frame and step scans were collected with rotation of the cell of ±38º with a typical exposure time of 0.5-2 s per frame.

The indexing of Bragg reflections, the intensity data reduction, and the empirical absorption correction were performed using the Agilent CrysAlisPro software (Oxford Diffraction 2006). Crystal structures were refined using Jana 2006 (Petricek et al. 2014). Polyhedral volumes were calculated using VESTA software (Momma and Izumi 2011). The Birch-Murnaghan and Vinet equations of state coefficients were refined using the program EoSFit-7c (Angel et al. 2014).

## Results

*In situ* X-ray diffraction experiments were performed up to 40 GPa for Na-Ti Px and up to 30 GPa for Fe-bearing Na-Mg-Si Px; the pressure-volume (*P*-*V*) data are given in Table S1 (Supplementary Information).

As shown in Figure 2, the Birch's normalized stress (FE)—Eulerian strain (*f*E) plots for both pyroxenes can be clearly fitted with horizontal straight lines. Therefore, the data can be fitted with a 2nd-order BM EoS. From this fitting, the bulk modulus obtained at room temperature is $K_0$ = 106.8(2) GPa for Na-Ti Px and $K_0$ = 121.8(4) GPa for Fe-bearing Na-Mg-Si Px. This is in a good agreement with the *P*-*V* data on the initial volume $V_0$ and room temperature bulk modulus $K_0$ for studied pyroxenes (Table 1). The normalized unit-cell parameters for pyroxenes calculated as $X_P/X_0$ ($X_P$ are the experimentally determined parameters *a*, *a*sinβ, *b*, *c* at pressure point *P*; $X_0$ = EoS values at ambient pressure) are shown in Figure 3. For a monoclinic mineral, in which the beta angle changes significantly with pressure, the *a*- and *c*-crystal axes are not the principal axes of the strain tensor, and, therefore, are not the directions of minimum and maximum compression in the crystal structure. Strain tensor of the mineral and the minimum and maximum compression direction in the *a*-*c* plane (Table S2 in Supplementary Information) were simulated with the cell-parameter data between room and pressure conditions using the win_strain software (http://www.rossangel.com/text_strain.htm). The unit strain ellipsoid is significantly anisotropic, as is demonstrated by the axial ratios ε1:ε2:ε3 = 1:3.07:1.64 (computed between 0–40.3 GPa), where ε2 is parallel to the *b* axis, ε1 and ε3 lie in the ac-plane perpendicular to each other and ε1 divides β. Neither the crystallographic *a* nor *c* axes are principal axes of the strain ellipsoids. The stiffest direction lies between +*a* and +*c*, since the β angle is changing as *P* increases, thus, contributing an expansion to directions between +*a* and +*c*. The stiffest direction in the structure of the studied pyroxenes lies close to the bisector of the obtuse angle β not along [101], but along [u0w] in the (010) plane at low pressures (Table S2 in Supplementary Information). As a function of pressure, we can see the change in the

value of the unit strain parallel to the stiffest direction and a significant change in its orientation, which is rotated counterclockwise. Thus, with increasing pressure, the stiffest direction lies close to [405]. As it was noted above, the *b* direction or [010] is the most compressible direction in studied pyroxenes. The kinking of the tetrahedral chains accounts for most of the anisotropy of compression observed in the *a*-*c* plane in particular along the ε1 (Thompson and Downs 2008).

Results of the structural refinements for studied pyroxenes are given in CIFs in Supplementary Information. The crystal structures of Fe-bearing Na-Mg-Si pyroxene and Na-Ti pyroxene are quite similar and based on three types of polyhedra: one octahedra ($M1O_6$), one eight-fold coordinated site ($M2O_8$) and one tetrahedron ($SiO_4$) (Fig. 4).

Within a coordination sphere of 2.6 Å, the M2 site is surrounded by six O atoms with two O3 atoms at a distance of 2.9 Å from the M2 cation. Since this value is significantly reduced to 2.32 Å for Na-Ti Px and to 2.39 Å for Fe-bearing Na-Mg-Si Px with increasing pressure, the coordination of the M2 site appears to become eightfold at $P$ > 20 GPa, whereas other Na-bearing pyroxenes still exhibit an octahedrally-coordinated M2 site (e.g., Prewitt and Burnham 1966; Clark et al. 1969; Ohashi et al. 1982). Fig. 5 shows that the effective coordination number changes as a function of pressure. In order to compare the effective coordination number in the $P$-range investigated it was fixed to the dodecahedral shape. M2 sites are distorted and occupied by Na with a small admixture of Mg and $Fe^{2+}$. The M1 sites are smaller and almost regular octahedral. The M1 site is occupied by Ti and Mg in Na-Ti Px, whereas this site for Fe-bearing Na-Mg-Si pyroxene is occupied by $Si^{4+}$, $Fe^{2+}$ and $Mg^{2+}$. The $SiO_4$ tetrahedra are connected via bridging O3 atoms to form chains running along the **c** axis. The $SiO_4$ tetrahedra are distorted: the Si–O bond distances range broadly from 1.53 to 1.66 Å with the Si–O3

bond being the longest one (Figs. 6c and 7c). The quadratic elongation and angular variation parameters (Robinson et al. 1971) have been used to determine the non-ideality of the coordination polyhedra.

With increasing pressure, all structural units show an anisotropic distortion. Figure 8 illustrates the normalized polyhedral volume for $M1O_6$, $M2O_8$, and $SiO_4$ polyhedra in studied pyroxenes.

The polyhedral volumes show clear changes with increasing pressure as well. A third-order Birch-Murnaghan EoS was used for the fitting of polyhedral volumes. For Na-Ti Px, between 3 and 40 GPa, the volume of $M1O_6$ decreases slightly from 10.9 to 8.97 $Å^3$ (Fig. 8a, Table s3) with a bulk modulus of 102(2) GPa. The evolution of the individual M1–O bonds is anisotropic (Fig. 8) with the following compressibility scheme: $\beta(M1–O1) = 2.9\times10^{-3}$ $GPa^{-1}$ > $\beta(M1–O2) = 2.4\times10^{-3}$ $GPa^{-1}$ >> $\beta(M1–O1) = 1.67\times10^{-3}$ $GPa^{-1}$. The Fe-bearing Na-Mg-Si Px is characterized by the similar compressibility scheme. In the pressure range from 4–30 GPa, the $M1O_6$ volume decreases from 10.27 to 9.111 $Å^3$ (Fig. 8b, Table s6) with a bulk modulus of 156(19) GPa indicating the following compressibility scheme: $\beta(M1–O1) = 3.46\times10^{-3}$ $GPa^{-1}$ > $\beta(M1–O2) = 2.4\times10^{-3}$ $GPa^{-1}$ >> $\beta(M1–O1) = 1.11\times10^{-3}$ $GPa^{-1}$.

The $M2O_8$ polyhedron with the bulk modulus of 73(1) GPa is much softer than M1. The studied pyroxenes are characterized by the following compressibility scheme: $\beta(M2–O3) >> \beta(M2–O1) \approx \beta(M2–O2) > \beta(M2–O3)$.

The Si-tetrahedron is the most rigid structural unit of the pyroxene structure (e.g. Yang and Prewitt, 2000). For Na-Ti Px in the pressure range from 3 to 40 GPa, its volume decreases from 2.137 to 2.028 $Å^3$ with a bulk modulus of 901(495) GPa. However, Fe-bearing Na-Mg-Si Px shows greater decrease in the Si-tetrahedron volume.

Between 4 and 30 GPa, its volume decreases from 2.13 to 1.90 $Å^3$ with a bulk modulus of 236(134) GPa. The Si-O1, Si-O2 and Si-O3 bonds show compressibilities of $\sim 1 \times 10^{-3}$ $GPa^{-1}$.

The characteristic feature of Na- pyroxenes is the decrease of the O3-O3-O3 angle from 171.9° at 3 GPa to 153.61° at 40 GPa for Na-Ti Px and from 172.2° at 4 GPa to 166° at 30 GPa for Fe-bearing Na-Mg-Si Px, which indicates a strong compression of tetrahedral chains (Table s5). It should be noted that most likely we observe an isostructural (isosymmetric) phase transition at around 22 GPa due to the rotation of the tetrahedral chains. The main change associated with the tetrahedral chains is the change in kinking, due to the decrease in the O3-O3-O3 angle from 22 GPa. Such rotation provokes the rapid increase in coordination of the M2 cations (Fig. 6b) from 6 to 8. The second-order isosymmetric phase transition has been also observed in aegirine at 24 GPa by Xu et al. (2017) with an evident discontinuity in the O3-O3-O3 angle at that pressure. Figure 6b shows the sympathetic M2–O3 bonds, which positioned to favor the tetrahedral rotation upon compression, and antipathetic M2–O3 bonds positioned to resist the rotation (McCarthy et al. 2008). The antipathetic M2–O3 bonds decrease much more slowly than the other M2–O3 bonds, since tetrahedral rotation provides a component of the O3 displacement away from M2. The antipathetic M2–O3 bonds have the smallest decrease with pressure while the sympathetic M2–O3 bonds have the greatest decrease.

## DISCUSSION

It is worthy to note that in contrast to Na-Ti Px, Fe-bearing Na-Mg-Si Px, as well as the starting material $Na(Mg_{0.5}Si_{0.5})Si_2O_6$ used for its synthesis, are the phases which contain both tetrahedrally and octahedrally coordinated silicon. A systematic survey of

these high-pressure structures (Finger and Hazen 2000; Pushcharovsky 2004) showed that besides pyroxenes, the silicates of the titanite, garnet (majorite), wadeite, benitoite and spinel structural types belong to this group. In addition, there are Na- and Mg-silicates with silicon in mixed four- and six-fold coordination. In experiments, all of them crystallize at pressures between about 5 and 20 GPa.

Based on the foregoing, it follows that the compressibility of Na-Ti Px (106.8(2) GPa) is significantly higher than that of Fe-bearing Na-Mg-Si Px (121.8(4) GPa). Fig. 13 shows comparison of unit cell volumes with increasing pressure for the two pyroxenes studied.

Dymshits et al. (2015) conducted a study of the compressibility of Na-rich pyroxene. In connection with the findings of Tribaudino et al. (2001), who showed that the M2 site chemistry has a little effect on the bulk modulus of pyroxenes, the relationship between the ambient unit-cell volume and M1 cation radius suggests that bulk compressibility in *C*2/*c* silicate pyroxenes may be controlled by the compressibility of the M1 octahedron. Thus, we should compare our results not only with high-Na pyroxenes, but also with other pyroxenes with similar structural characteristics. The compressibility systematics of clinopyroxenes has been a subject of intensive research. Several factors responsible for the bulk moduli variation have been proposed: volume-bulk modulus systematic at ambient conditions (Bridgman 1923), cation size and occupancy of the M1 site (Thompson and Downs 2004), type (sympathetic or antipathetic) of the M2-O3 bonds (McCarthy et al. 2008).

Thompson et al. (2005) showed that the unit cell volume is largely a function of M1, and the bulk modulus of *C*2/*c* pyroxenes depends primarily on the occupancy of the M1 site. The bulk moduli values of Na-Ti- and Na-Mg-Si Px (106.8(2) and 121.8(4) GPa,

299 respectively) indicate that the substitution of $Mg^{2+}$ cation ($r(Mg^{2+})$=0.72 Å) with the
300 slightly larger $Fe^{2+}$ cation ($r(Fe^{2+})$=0.78 Å) at the M1 site causes softening of the *C*2/*c*
301 structure. Such behavior was observed for olivine (Zhang et al. 1997), and the Fe-Mg
302 spinel solid solution (Hazen 1993) as well. In addition, we can see the effect of $Fe^{2+}$ on
303 pyroxene compressibility by comparing the *C*2/*c* Fe-bearing Na-Mg-Si Px (this study)
304 and *P*2/*n* pyroxene with the composition $NaMg_{0.5}Si_{2.5}O_6$ (Dymshits et al. 2015). The bulk
305 moduli of $NaMg_{0.5}Si_{2.5}O_6$ pyroxene is 103(2), which is significantly lower than that of
306 Fe-bearing Na-Mg-Si Px (121.8(4) GPa). The stiffer structure is typical of pyroxenes
307 with Mg substitution with $Fe^{3+}$ in the octahedral M1 site ($r(Fe^{3+})$=0.64 Å), $Al^{3+}$
308 ($r(Al^{3+})$=0.535 Å) and $Cr^{3+}$($r(Cr^{3+})$=0.615 Å); their bulk moduli are 117.9(4), 136.5(14),
309 136.7(6), respectively. The increased stiffness of such pyroxenes may indicate their lower
310 transition pressures in comparison with $NaMg_{0.5}Si_{2.5}O_6$ or $Na(Mg_{0.5}Ti_{0.5})Si_2O_6$.
311 Incorporation of $Ti^{4+}$ in the M1 site does not influence on the bulk modulus of pyroxene.
312 It is shown that the type of the M2-O3 bonds (sympathetic or antipathetic) is very
313 important as well. The M2-O3 bonds display one of two behavior modes as pyroxene
314 structures are compressed and $SiO_4$ tetrahedra rotate, which results in change of the O3-
315 O3-O3 angles and decrease in M2-O3 distances (Downs 2003). The M2-O3 bonds with
316 decreasing length are inhibited by the pressure-induced tetrahedral rotation, which tends
317 to resist rotation, and are, thus, termed “antipathetic” bonds typical of diopside and other
318 Ca-rich pyroxenes. “Antipathetic” bonds are positioned to resist the tetrahedral rotation.
319 In contrast, the M2-O3 bonds that are further shortened by tetrahedral rotation would
320 either assist or have no effect on tetrahedral rotation, and are thus termed “sympathetic”
321 bonds.

M2 in the structures of our *C*2/*c* Na-rich pyroxenes and *P*2/*n* Na-pyroxene described by Dymshits et al. (2015) has two (topologically identical) antipathetic and two sympathetic M2-O3 bonds; this is characteristic of all *C*2/*c* pyroxenes, in which the M2 site is eight-fold and bonded to all bridging O atoms. The group of monovalent-M2 *C*2/*c* pyroxenes ($LiAlSi_2O_6$, $NaAlSi_2O_6$, $NaCrSi_2O_6$, and $NaFeSi_2O_6$), in which M2 is six-fold and bonded to two bridging O atoms, is characterised by the presence of antipathetic M2-O3 bonds. Figures 6b and 10b shows the change in M2-O distances in our Na-rich pyroxenes as a function of pressure. It was found that the antipathetic M2-O3 bonds decreased in length much more slowly than the other M2-O bonds, since tetrahedral rotation provided a component of O3 displacement away from M2. The antipathetic M2-O3 distance shows the smallest decrease with pressure, while the sympathetic M2-O3 distance has the greatest decrease. This can be interpreted by coupling of the common compression of the structure with pressure and rotation of the silicate tetrahedra, which leads to shortening or lengthening of some interatomic distances. Thus, pyroxenes with only antipathetic M2-O3 bonds are much stiffer in comparison with phases containing two types of bonds.

McCarthy et al. (2008) predicted that the bulk moduli of silicate clinopyroxenes with antipathetic M2–O3 bonds should follow $K_0^{ant}$ (GPa) = $-0.5051V_0$ (Å$^3$) + 339.37, whereas clinopyroxenes without antipathetic M2–O3 bonds should follow $K_0^{sym}$ (GPa) = $-0.7784V_0$ (Å$^3$) + 419.14. At the same time, it was suggested that the effect of temperature should not be significant. Thus, Cameron et al. (1973) found that the expansion of the jadeite structure from ambient temperature to 800ºC resulted in increase in the unit cell volume by 1.9% only, and increase in pressure up to 9 GPa reduced the unit cell volume by 5.9%. In this study, we show that the unit cell volume of Na-Ti-Px

346 decreases by 20.9% with increasing pressure up to 40 GPa, and the unit cell volume of
347 Na-Mg-Si Px decreases by 15.8% with increasing pressure within the range of 0–30 GPa.
348 Our Na-rich pyroxenes and *P*2/*n* $NaMg_{0.5}Si_{2.5}O_6$ pyroxene (Dymshits et al., 2015) are in
349 an intermediate position between pyroxenes with two anthypathetic M2–O3 bonds (upper
350 trend) and pyroxenes with only sympathetic M2–O3 bonds (lower trend) (Fig. 14). This
351 fact indicates that the bulk modulus of such pyroxenes with different compositions can be
352 calculated, and these values can vary within the $K_0^{ant} - K_0^{sym}$ range.
353

354 **Implications**

355

356 Despite significant interest of experimentalists to the study of geophysically
357 important phase equilibria in the Earth's mantle and the need to increase the experimental
358 database related to multicomponent systems, incorporation of Si and $Ti^{4+}$ in the
359 octahedral sites of minerals is very important for understanding the processes in the deep
360 Earth and in obtaining the data on the composition and structure of deep Earth
361 geospheres. The influence of these elements on structural peculiarities of high-pressure
362 phases may have a certain impact on the *PT*-parameters and phase transformations.
363 Si-rich Na-pyroxene and Na-majorite (Dymshits et al. 2010; Bindi et al. 2011)
364 have the same chemical compositions and should be considered as potential hosts for
365 sodium in the Earth's upper mantle areas characterized by an excess of Na with respect to
366 Al in the bulk. Generally, this is not typical of peridotitic lithologies in the upper mantle
367 regularly sampled by mantle xenoliths. However, the probability to find a Na-rich
368 substrate in the deep mantle is confirmed by an inclusion in diamond with the
369 composition of $(Na_{0.16}Mg_{0.84})(Mg_{0.92}Si_{0.08})Si_2O_6$ found in a kimberlite from China (Wang

and Sueno 1996). As this phase has been found to have the garnet structure (Wang and Gasparik, 2000), the appropriate compositions should exist in the mantle to stabilize Na-pyroxene as a component in pyroxene below the pyroxene–garnet transition pressure, which is approximately 16.5 GPa (Gasparik 1989). Our studies have shown that incorporation of small amount of $Fe^{3+}$ to Na-pyroxene significantly increases both the bulk modulus and the pressure of the Na-Px/Na-Grt transformation. Previously, the pyroxene/garnet phase transition in the $Na_2MgSi_5O_{12}$ was studied in a wide range of *P–T* parameters (14–18 GPa, 1500–2100°C; Dymshits et al. 2010; 2013). These authors have shown that at 15 GPa and 1500 °C (which corresponds to the synthesis conditions of Fe-bearing Na-Mg-Si pyroxene in this study) Na-Maj is stable.

The formation of most of Na-rich minerals and phase assemblages in the Earth's mantle is related to crystallization of alkaline carbonate-silicate melts (Bobrov et al. 2008). Such melts (Klein-BenDavid et al. 2006) are known from inclusions in diamonds and are considered to be the most active agents of mantle magmatism and metasomatism, as well as diamond formation. Walter et al. (2008) suggested that melting occurred due to the crust-mantle interaction as slabs descended to the mantle and stagnated in the transition zone being heated up to the carbonated eclogite solidus where they released a low-degree melt.

Similarly, titanium-rich lithologies in the Earth's mantle are caused by the crust-mantle interaction and subduction of the oceanic crust containing MORB with ~2 wt% $TiO_2$ to different depths (Sours-Page et al. 1999). The new Na-Ti-pyroxene was synthesized at the upper mantle pressure (7 GPa) (Sirotkina et al. 2016). Unfortunately, there is still no data on Na-Ti pyroxene/Na-Ti garnet or Na-Ti pyroxene/Ti-bridgmanite phase transitions. It has also been shown that Ti stabilizes the bridgmanite structure to

lower pressure regions, so that Ti-bearing bridgmanite may be stable at pressures above 18 GPa (Bindi et al. 2017). Inclusions in some superdeep natural diamonds provide evidence for Ti-rich domains at transition zone depths that are likely related to metasomatism by low-degree melts (e.g., Thomson et al. 2016). The Ti-rich phases are potentially stable in such Ti-rich environments, where the high content of titanium and presence of high-Ti phases could have important geochemical effects or act as a tracer for metasomatic processes.

Further work is needed to determine the *PT*-parameters of stability of these titanium-rich phases, and to determine their thermo-physical and chemical properties.

## ACKNOWLEDGMENTS

Constructive reviews of three anonymous referees were very helpful for improving the quality of the manuscript. We acknowledge the ESRF and DESY for provision of synchrotron radiationfacilities. This study was supported by the Russian Science Foundation (project no. 17-17-01169 to AB, EM, and LI). The structural refinement of Na-Ti pyroxene was supported by the Foundation of the President of the Russian Federation (grant no. MK-1277.2017.5 to EM). The comparison of the structures of synthesized pyroxenes with the phases available from literature - by the Russian Foundation of Basic Research (grant no. 18-05-00332 to DP).

## References

Angel, R. J. Win_Strain program for Strain calculations. (http://www.rossangel.com/text_strain.htm). 2011.

Angel, R. J. (2000) Equations of state. Reviews in Mineralogy and Geochemistry, 41(1), 35-59.

Angel, R.J., Gasparik, T., Ross, N.L., Finger, L.W., Prewitt, C.T., and Hazen, R.M. (1988) A silica-rich sodium pyroxene phase with six-coordinated silicon. Nature, 335,156 -158.

Arlt, T., and Angel, R.J. (2000) Displacive phase transitions in C-centred clinopyroxenes: spodumene, $LiScSi_2O_6$ and $ZnSiO_3$. Physics and Chemistry of Minerals, 27(10), 719-731.

Aulbach, S., Griffin, W. L., Pearson, N. J., O'Reilly, S. Y., Kivi, K., and Doyle, B. J. (2004) Mantle formation and evolution, Slave Craton: constraints from HSE abundances and Re–Os isotope systematics of sulfide inclusions in mantle xenocrysts. Chemical Geology, 208(1-4), 61-88.

Bindi, L., Dymshits, A.M., Bobrov, A.V., Litasov, K.D., Shatskiy, A.F., Ohtani, E., and Litvin, Yu.A. (2011) Crystal chemistry of sodium in the Earth's interior: The structure of $Na_2MgSi_5O_{12}$ synthesized at 17.5 GPa and 1700 C. American Mineralogist, 96(2-3), 447-450.

Bishop, F.C., Smith, J.V., and Dawson, J.B. (1978) Na, K, P and Ti in garnet, pyroxene and olivine from peridotite and eclogite xenoliths from African kimberlites. Lithos, 11, 155–173.

Bobrov, A.V., Litvin, Yu.A., Bindi, L., and Dymshits, A.M. (2008) Phase relations and formation of sodium-rich majoritic garnet in the system $Mg_3Al_2Si_3O_{12}$–$Na_2MgSi_5O_{12}$ at 7.0 and 8.5 GPa. Contributions to Mineralogy and Petrology, 156, 243–257.

Bobrov, A.V., and Litvin, Yu.A. (2009) Peridotite–eclogite–carbonatite systems at 7.0–8.5 GPa: concentration barrier of diamond nucleation and syngenesis of its silicate and carbonate inclusions. Russian Geology and Geophysics, 50, 1221-1233.

443 Bridgman, P.W. (1923) The compressibility of thirty metals as a function of pressure and
444 temperature. Proceedings of the American Academy of Arts and Sciences, 58,
445 165–242.
446 Cameron, M., and Papike, J.J. (1981) Structural and chemical variations in pyroxenes.
447 American Mineralogist, 66(1-2), 1-50.
448 Cameron, M., Sueno, S., Prewitt, C.T., and Papike, J.J. (1973) High temperature crystal
449 chemistry of acmite, diopside, hedenbergite, jadeite, spodumene, and ureyite.
450 American Mineralogist, 58, 594-618.
451 Clark, J.R., Appleman, D.E., and Papike, J.J. (1969) Crystal-chemical characterization of
452 clinopyroxenes based on eight new structure refinements. MSA Special Paper, 2,
453 31-50.
454 Downs, R.T. (2003) Topology of the pyroxenes as a function of temperature, pressure
455 and composition determined from the procrystal electron density. American
456 Mineralogist, 88, 556–566
457 Dymshits, A., Sharygin, I., Litasov, K., Shatskiy, A., Gavryushkin, P., Ohtani, E., Suzuki,
458 A., and Funakoshi, K. (2015). In situ observation of the pyroxene-majorite
459 transition in $Na_2MgSi_5O_{12}$ using synchrotron radiation and Raman spectroscopy of
460 Na-majorite. American Mineralogist, 100(2-3), 378-384.
461 Dymshits, A.M., Bobrov, A.V., Bindi, L., Litvin, Y.A., Litasov, K.D., Shatskiy, A.F., and
462 Ohtani, E. (2013) Na-bearing majoritic garnet in the $Na_2MgSi_5O_{12}$–$Mg_3Al_2Si_3O_{12}$
463 join at 11–20 GPa: Phase relations, structural peculiarities and solid solutions.
464 Geochimica et Cosmochimica Acta, 105, 1–13.
465 Dymshits, A.M., Bobrov, A.V., Litasov, K.D., Shatskiy, A.F., Ohtani, E., and Litvin,
466 Yu.A. (2010) Experimental study of the pyroxene-garnet phase transition in the

$Na_2MgSi_5O_{12}$ system at pressures of 13–20 GPa: First synthesis of sodium majorite. Doklady Earth Sciences, 434, 1263–1266.

Fei, Y., Ricolleau, A., Frank, M., Mibe, K., Shen, G., and Prakapenka, V. (2007) Toward an internally consistent pressure scale. Proceedings of the National Academy of Sciences U.S.A., 104, 9182-9186.

Finger, L.W., and Hazen, R.M. (2000). Systematics of high-pressure silicate structures. Reviews in Mineralogy and Geochemistry, 41(1), 123-155.

Frost, D.J., Poe, B.T., Trønnes, R.G., Liebske, C., Duba, A., and Rubie, D. C. (2004), A new large-volume multianvil system. PhysIcs of the Earth and Planetary Interiors, 143–144, 507–514.

Gasparik, T. (1988) The synthesis of a new pyroxene-$NaMg_{0.5}Si_{2.5}O_6$ and garnet near the diopside–jadeite join. Eos Transactions, 69, 500.

Gasparik, T. (1989) Transformation of enstatite – diopside – jadeite pyroxenes to garnet. Contributions to Mineralogy and Petrology, 102(4), 389–405.

Gatta, G.D., Ballaran, T.B., and Iezzi, G. (2005) High-pressure X-ray and Raman study of a ferrian magnesian spodumene. Physics and Chemistry of Minerals, 32(2), 132-139.

Hazen, R.M. (1993) Comparative compressibilities of silicate spinels: Anomalous behavior of $(Mg,Fe)_2SiO_4$. Science, 259, 206-209.

Hazen, R.M., and Finger, L.W. (1977). Crystal structure and compositional variation of Angra dos Reis fassaite. Earth and Planetary Science Letters, 35(2), 357-362.

Klein-BenDavid, O., Wirth, R., and Navon, O. (2006) TEM imaging and analysis of microinclusions in diamonds: A close look in diamond-growing fluids. American Mineralogist, 91, 353–365.

Levien, L., and Prewitt, C.T. (1981) High-pressure structural study of diopside. American Mineralogist, 66(3-4), 315-323.

McCarthy, A.C., Downs, R.T., and Thompson, R.M. (2008) Compressibility trends of the clinopyroxenes, and in situ high-pressure single-crystal X-ray diffraction study of jadeite. American Mineralogist, 93, 198–209.

Momma, K., and Izumi, F. (2011) VESTA 3 for three-dimensional visualization of crystal, volumetric and morphology data. Journal of Applied Crystallography, 44(6), 1272-1276.

Nestola, F., Ballaran, T. B., Liebske, C., Bruno, M., and Tribaudino, M. (2006) High-pressure behaviour along the jadeite $NaAlSi_2O_6$–aegirine $NaFeSi_2O_6$ solid solution up to 10 GPa. Physics and Chemistry of Minerals, 33(6), 417-425.

Nestola, F., Boffa Ballaran, T., Liebske, C., Thompson, R., and Downs, R.T. (2008) The effect of the hedenbergitic substitution on the compressibility of jadeite. American Mineralogist, 93(7), 1005-1013.

Ninomiya, E., Isobe, M., Ueda, Y., Nishi, M., Ohoyama, K., Sawa, H., and Ohama, T. (2003) Observation of lattice dimerization in spin singlet low temperature-phase of $NaTiSi_2O_6$. Physica B, 329, 884–885.

Ohashi, H., Fujita, T., and Osawa, T. (1982) The crystal structure of $NaTiSi_2O_6$ pyroxene. The Journal of the Japanese Association of Mineralogists, Petrologists and Economic Geologists, 77, 305–309.

Petricek, V., Dusek, M., and Palatinus, L. (2014) Crystallographic Computing System JANA2006: General features. Zeitschrift für Kristallographie-Crystalline Materials, 229, 345.

514 Prewitt, C.T., Shannon, R.D., and White, W.B. (1972) Synthesis of a pyroxene
515 containing trivalent titanium. Contributions to Mineralogy and Petrology, 35, 77–
516 82.
517 Prewitt, C.T., and Burnham, C.W. (1966) The crystal structure of jadeite, $NaAlSi_20_6$.
518 American Mineralogist, 51, 956-975.
519 Pushcharovsky, D.Yu. (2004) Mineral transformation processes in deep geospheres.
520 Moscow University Geology Bulletin, 59(2), 1-11.
521 Redhammer, G.J., Ohashi, H., and Roth, G. (2003) Single-crystal structure refinement of
522 $NaTiSi_2O_6$ clinopyroxene at low temperatures (298<T<100 K). Acta
523 Crystallographica Section, B59(6), 730-746.
524 Rigaku, O. D. (2015) CrysAlis PRO. Rigaku Oxford Diffraction, Yarnton, England.
525 Robinson, K., Gibbs, G.V., and Ribbe, P.H. (1971) Quadratic elongation: a quantitative
526 measure of distortion in coordination polyhedra. Science, 172, 567-570.
527 Rudnick, R.L., Gao, S., Ling, W.L., Liu, Y.S., and McDonough W.F. (2004) Petrology
528 and geochemistry of spinel peridotite xenoliths from Hannuoba and Qixia, North
529 China craton. Lithos, 77(1), 609-637.
530 Sheldrick, G.M. (2008) A short history of SHELX. Acta Crystallographica, A64, 112.
531 Sirotkina, E. A., Bobrov, A. V., Spivak, A. V., Bindi, L., and Pushcharovsky, D. Yu.
532 (2016) X-ray single-crystal and Raman study of $(Na_{0.86}Mg_{0.14})(Mg_{0.57}Ti_{0.43})Si_2O_6$,
533 a new pyroxene synthesized at 7 GPa and 1700° C. Physics and Chemistry of
534 Minerals, 43(7), 731-738.
535 Sours-Page, R., Johnson, K. T., Nielsen, R. L., and Karsten, J. L. (1999) Local and
536 regional variation of MORB parent magmas: evidence from melt inclusions from

the Endeavour Segment of the Juan de Fuca Ridge. Contributions to Mineralogy and Petrology, 134(4), 342-363.

Stixrude, L., and Lithgow-Bertelloni, C. (2005) Mineralogy and elasticity of the oceanic upper mantle: origin of the low-velocity zone. Journal of Geophysical Research: Solid Earth, 110, B03204.

Thompson, R. M., and Downs, R. T. (2008) The crystal structure of diopside at pressure to 10 GPa. American Mineralogist, 93(1), 177-186.

Thompson, R. M., Downs, R. T., and Redhammer, G. J. (2005). Model pyroxenes III: Volume of *C*2/*c* pyroxenes at mantle P, T, and x. American Mineralogist, 90(11-12), 1840-1851.

Thompson, R.M., and Downs, R.T. (2004) Model pyroxenes II: Structural variation as a function of tetrahedral rotation. American Mineralogist, 89, 614–628.

Ullrich, A., Miletich, R., Balič-Žunić, T., Olsen, L., Nestola, F., Wildner, M., and Ohashi, H. (2010) $(Na,Ca)(Ti^{3+},Mg)Si_2O_6$-clinopyroxenes at high pressure: influence of cation substitution on elastic behavior and phase transition. Physics and Chemistry of Minerals, 37, 25–43.

Walter, M.J., Bulanova, G.P., Armstrong, L.S., Keshav, S., Blundy, J.D., Gudfinnsson, G., and Gobbo, L. (2008) Primary carbonatite melt from deeply subducted oceanic crust. Nature, 454, 622-625.

Wang, W., and Gasparik, T. (2000) Evidence for a deep-mantle origin of a NaPx-En inclusion in diamond. International Geology Review, 42(11), 1000-1006.

Wang, W., and Sueno, S. (1996) Discovery of a NaPx–En inclusion in diamond: possible transition zone origin. Mineralogical Journal, 18(1), 9-16.

560 Xu, J., Zhang, D., Fan, D., Downs, R. T., Hu, Y., and Dera, P. K. (2017) Isosymmetric
561 pressure-induced bonding increase changes compression behavior of
562 clinopyroxenes across jadeite-aegirine solid solution in subduction zones. Journal
563 of Geophysical Research: Solid Earth, 122(1), 142-157.
564 Yang, H., and Konzett, J. (2005) Crystal chemistry of a high-pressure *C*2/*c* clinopyroxene
565 with six-coordinated silicon. American Mineralogist, 90(7), 1223-1226.
566 Yang, H., Konzett, J., Frost, D.J., and Downs, R.T. (2009) X-ray diffraction and Raman
567 spectroscopic study of clinopyroxenes with six-coordinated Si in the Na
568 $(Mg_{0.5}Si_{0.5})Si_2O_6$-$NaAlSi_2O_6$ system. American Mineralogist, 94(7), 942-949.
569 Yang, H., and Prewitt, C.T. (2000) Chain and layer silicates at high temperatures and
570 pressures. Reviews in Mineralogy and Geochemistry, 41(1), 211-255.
571 Zhang, L., Ahsbahs, H., Hafner, S.S., and Kutoglu, A. (1997) Single-crystal compression
572 and crystal structure of clinopyroxene up to 10 GPa. American Mineralogist, 82(3-
573 4), 245-258.
574 Zhao, Y., Von Dreele, R.B., Shankland, T.J., Weidner, D.J., Zhang, J.Z., Wang, Y.B.,
575 and Gasparik, T. (1997) Thermoelastic equation of state of jadeite $NaAlSi_2O_6$: an
576 energy-dispersive Reitveld refinement study of low symmetry and multiple phases
577 diffraction. Geophysical Research Letters, 24, 5–8.
578

This is a preprint, the final version is subject to change, of the American Mineralogist (MSA)
Cite as Authors (Year) Title. American Mineralogist, in press.
DOI: https://doi.org/10.2138/am-2019-6658

579 **Table 1.** EoS coefficients resulting from the fits using a third-order Birch-Murnaghan
580 EoS for unit-cell parameters and volume for Na-Ti Px and Fe-bearing Na-Mg-Si Px

| | Birch-Murnaghan | |
|---|---|---|
| Composition | $V_0$ (Å$^3$) | $K_0$(GPa) |
| Na-Ti pyroxene | 428.57(20) | 106.8(2) |
| Fe-bearing Na-Mg-Si pyroxene | 413.20(4) | 121.8(4) |

581

This is a preprint, the final version is subject to change, of the American Mineralogist (MSA)
Cite as Authors (Year) Title. American Mineralogist, in press.
DOI: https://doi.org/10.2138/am-2019-6658

582 **Table 2.** Equation of state coefficients for unit-cell volumes for Na-bearing pyroxenes

| | Birch-Murnaghan | | | |
|---|---|---|---|---|
| Composition | $V_0$ (Å$^3$) | K (GPa) | K' | Ref. |
| Na-Ti | 428.57(20) | 106.8(2) | - | This study |
| Fe-bearing Na-Mg-Si | 413.20(4) | 121.8(4) | - | This study |
| $NaMg_{0.5}Si_{2.5}O_6$ | 407.2 | 103(2) | 6.2(7) | Dymshits et al. 2015 |
| $NaAlSi_2O_6$ (Jd) | 402.03(2) | 136.5(14) | 3.4(4) | McCarthy et al. 2008 |
| $NaAlSi_2O_6$ (Jd) | 402.26(2) | 134.0(7) | 3.7(6) | Nestola et al. 2006 |
| $NaFe^{3+}Si_2O_6$ (Aeg) | 429.25(3) | 116.1(5) | 4.4(1) | Nestola et al., 2006 |
| $NaFe^{3+}Si_2O_6$ (Aeg) | 429.40(9) | 117(1) | 3.2(2) | McCarthy et al. 2008 |
| $NaFe^{3+}Si_2O_6$ (Aeg) | 431.5(1) | 126(2) | 3.4(10) | Xu et al., 2017 |

583

584 FIGURE CAPTIONS

585 **Fig. 1.** (a) BSE image of an aggregate of euhedral Na–Ti-pyroxene crystals (light gray)
586 and in the quenched groundmass of elongate rutile (white) and pyroxene (light gray)
587 crystals (7 GPa, 1700°C); (b) SE image of Na-Mg-Si pyroxene aggregates in a
588 groundmass composed of very small pyroxene and stishovite grains (14 GPa, 1500°C)

589 **Fig. 2** Normalized pressure $F_E$ (GPa) – Eulerian strain $f_E$ plot for studied pyroxenes.

590 **Fig. 3.** Normalized unit cell parameters of studied pyroxenes.

591 **Fig 4.** The crystal structure of Na-Ti pyroxene at 3 GPa. Shown the configuration of O-
592 rotated tetrahedral chain with O3-O3-O3 angle of 171.9(8). Given are M1O6 octahedra
593 and SiO4 tetrahedra. The O3 atoms that can be bonded to M2 are labelled $O3_2$ and $O3_3$,
594 which are sympathetic and $O3_1$ and $O3_4$ which are antipathetic.

595 **Fig 5.** Effective coordination number for M2 site as a function of pressure for studied
596 pyroxenes

597 **Fig. 6.** Pressure dependence of the selected interatomic distances for Na-Ti Px. Pressure
598 measurement errors are less than symbol sizes.

599 **Fig. 7.** Pressure dependence of selected interatomic distances in Fe-bearing Na-Mg-Si
600 pyroxene. Pressure measurement errors are less than symbol sizes.

601 **Fig. 8.** Normalized polyhedral volume of studied pyroxenes

602 **Fig. 9.** Volume – pressure dependence for Na-rich pyroxenes. Errors are less than symbol
603 sizes. The results of fits using a $2^{nd}$-order Birch-Murnaghan equation of state are shown
604 by solid line.

605 **Fig. 10.** Dependence of the bulk modulus on the unit cell volume for $C2/c$ and $P2_1/c$
606 pyroxenes (Arlt and Angel 2000; Gatta et al. 2005; McCarthy et al. 2008). Bulk modulus

for Na-rich pyroxenes and *P*2/*n* $NaMg_{0.5}Si_{2.5}O_6$ pyroxene (Dymshits et al. 2015) vary within the $K_0^{ant} - K_0^{sym}$ range.

Figure 1

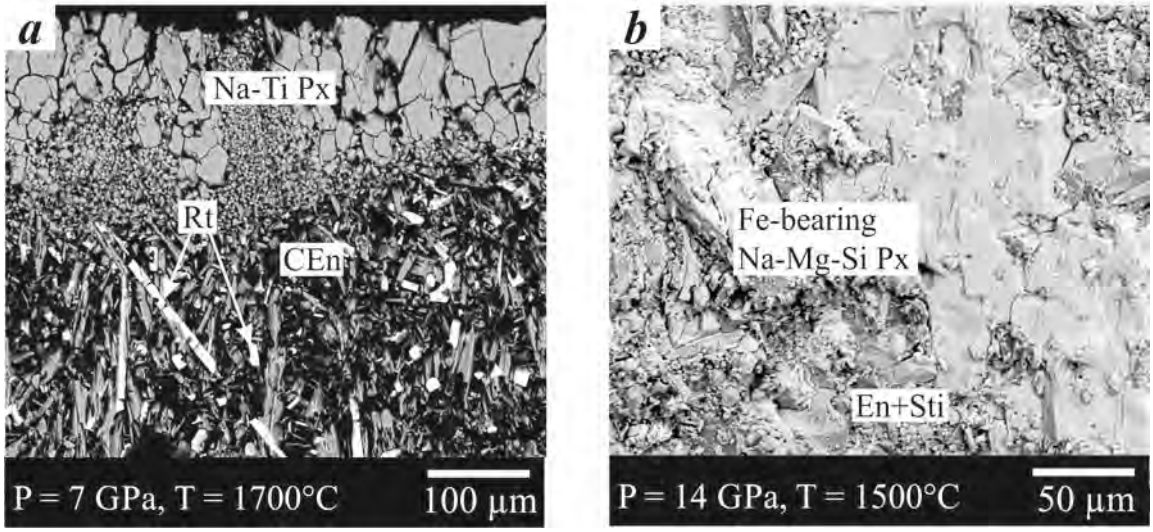
a
Na-Ti Px
Rt
CEn
P = 7 GPa, T = 1700°C
100 μm
b
Fe-bearing
Na-Mg-Si Px
En+Sti
P = 14 GPa, T = 1500°C
50 μm

Figure 2

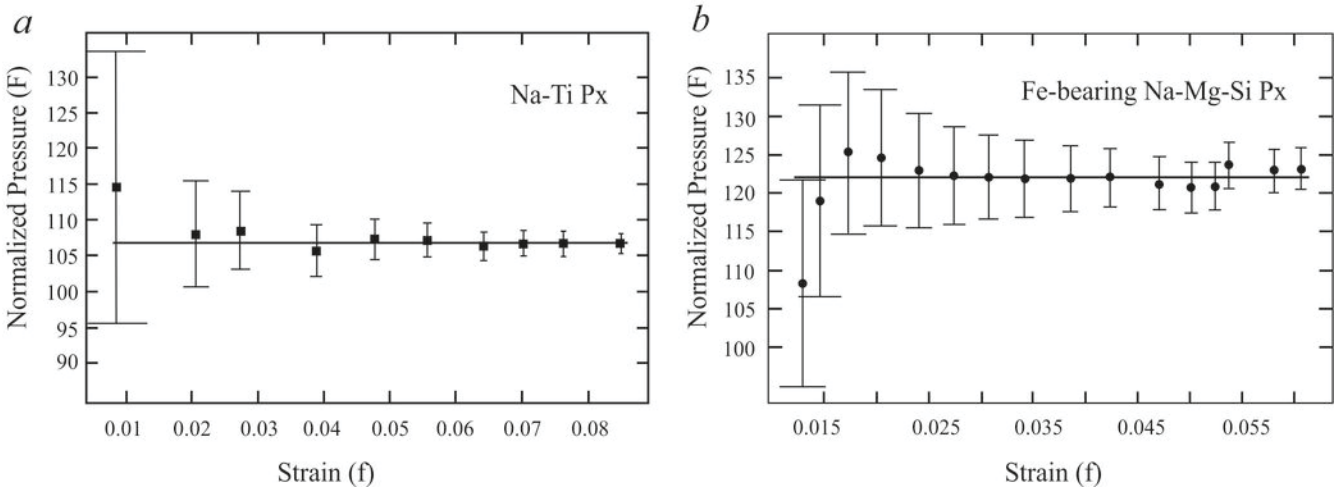
a
Na-Ti Px
Normalized Pressure (F)
130
125
120
115
110
105
100
95
90
0.01
0.02
0.03
0.04
0.05
0.06
0.07
0.08
Strain (f)
b
Fe-bearing Na-Mg-Si Px
Normalized Pressure (F)
135
130
125
120
115
110
105
100
0.015
0.025
0.035
0.045
0.055
Strain (f)

Figure 3

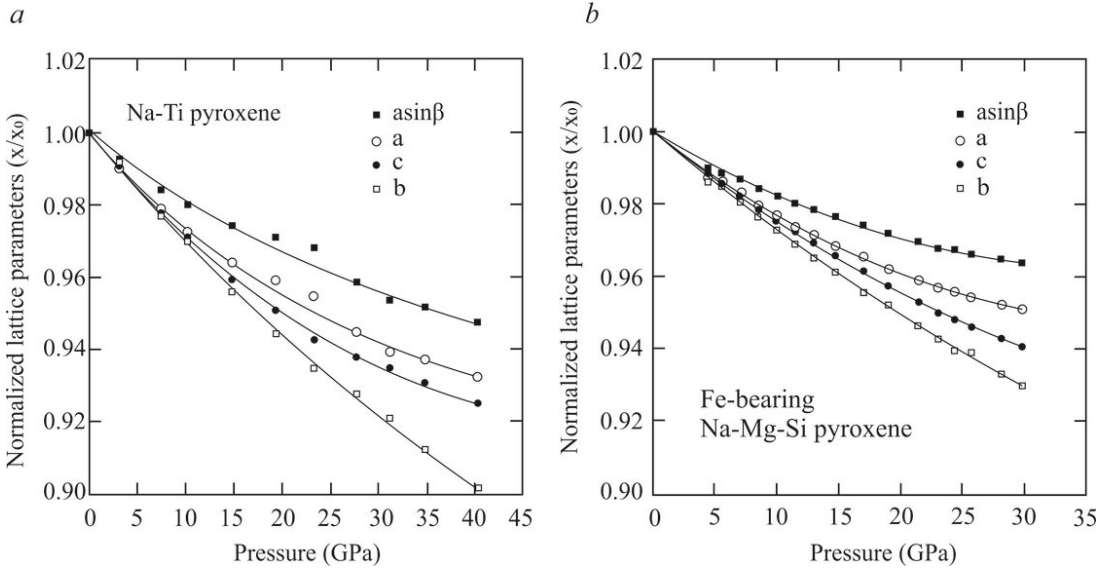
a
b
Na-Ti pyroxene
asinβ
a
c
b
Normalized lattice parameters (x/x0)
Pressure (GPa)
Fe-bearing
Na-Mg-Si pyroxene
1.02
1.00
0.98
0.96
0.94
0.92
0.90
0
5
10
15
20
25
30
35
40
45

Figure 4

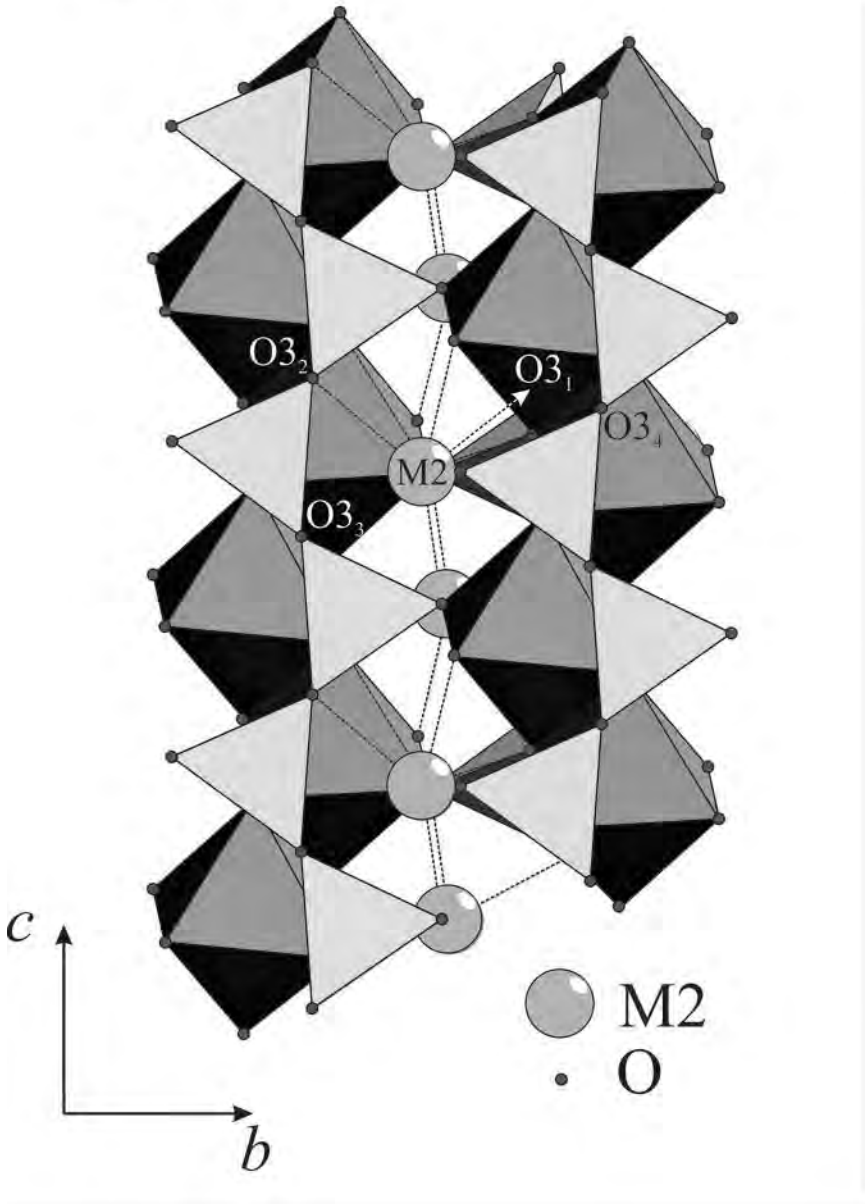

Figure 5

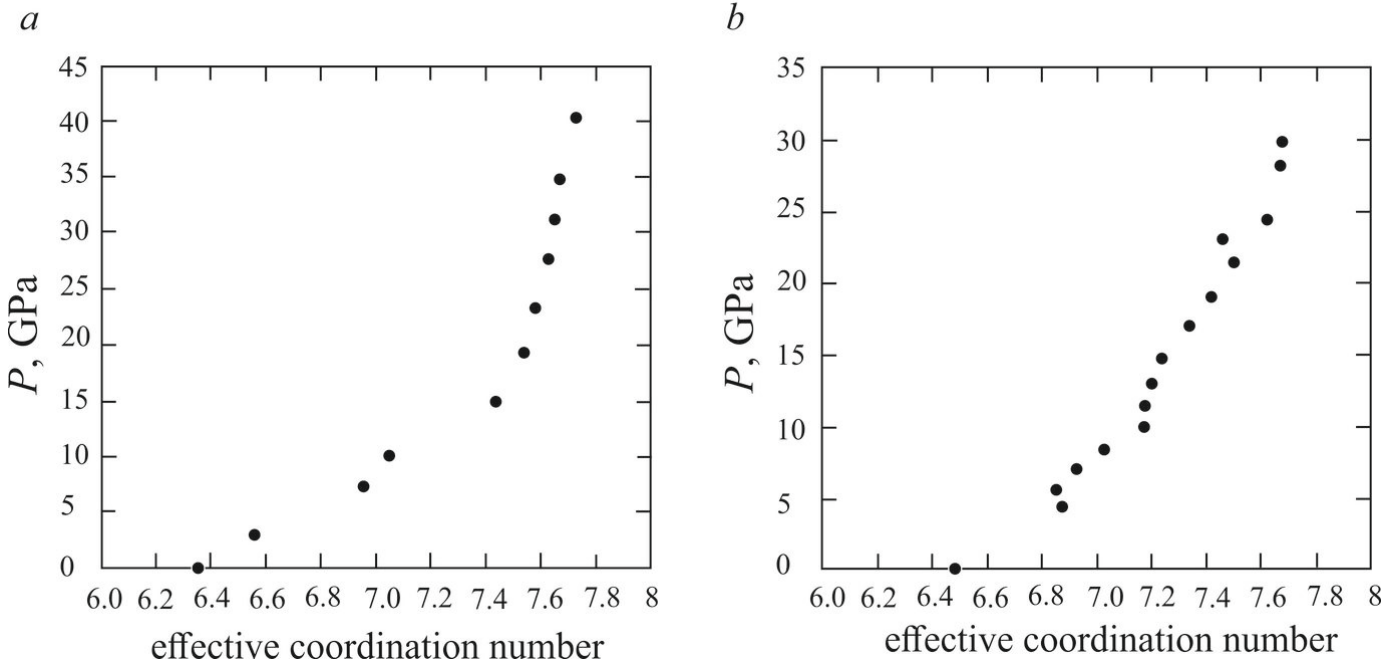
a
b
P, GPa
effective coordination number
0
5
10
15
20
25
30
35
40
45
6.0
6.2
6.4
6.6
6.8
7.0
7.2
7.4
7.6
7.8
8

Figure 6a

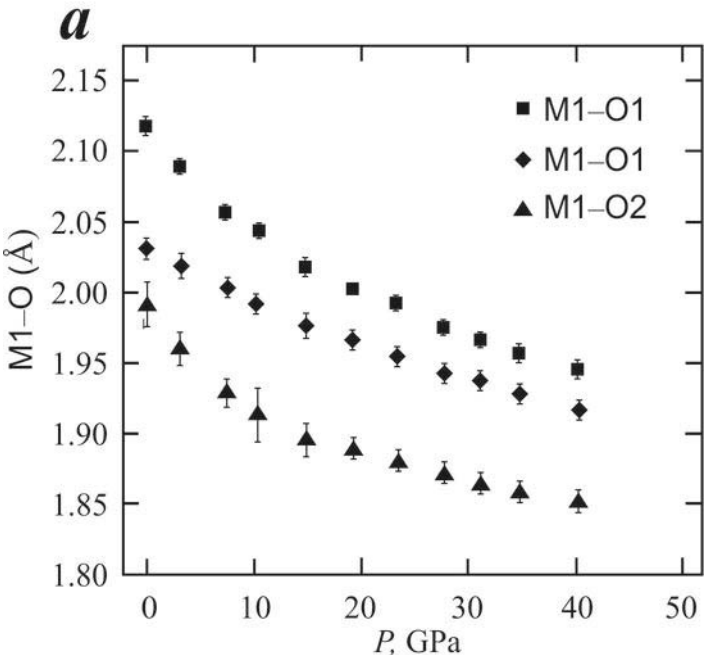
a
2.15
2.10
2.05
2.00
1.95
1.90
1.85
1.80
M1–O (Å)
0
10
20
30
40
50
P, GPa
M1–O1
M1–O1
M1–O2

Figure 6b

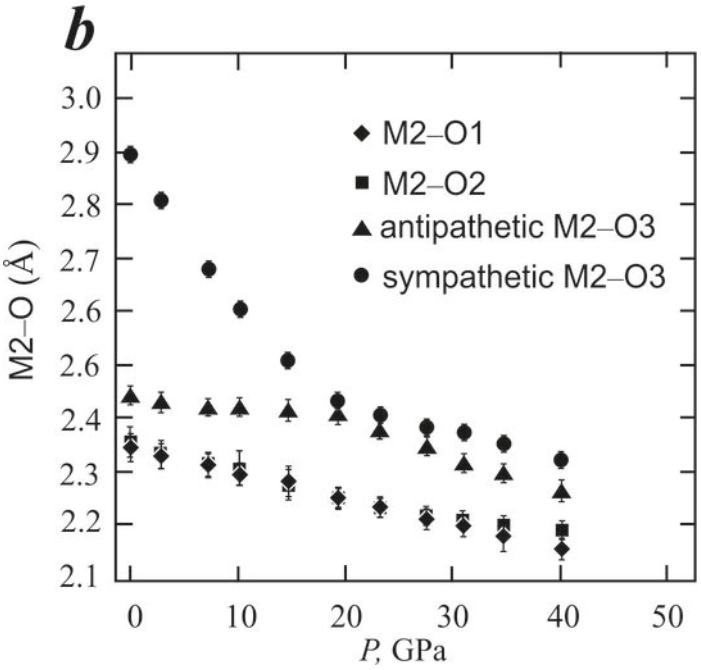
b
M2–O1
M2–O2
antipathetic M2–O3
sympathetic M2–O3
M2–O (Å)
P, GPa
3.0
2.9
2.8
2.7
2.6
2.6
2.4
2.3
2.2
2.1
0
10
20
30
40
50

Figure 6c

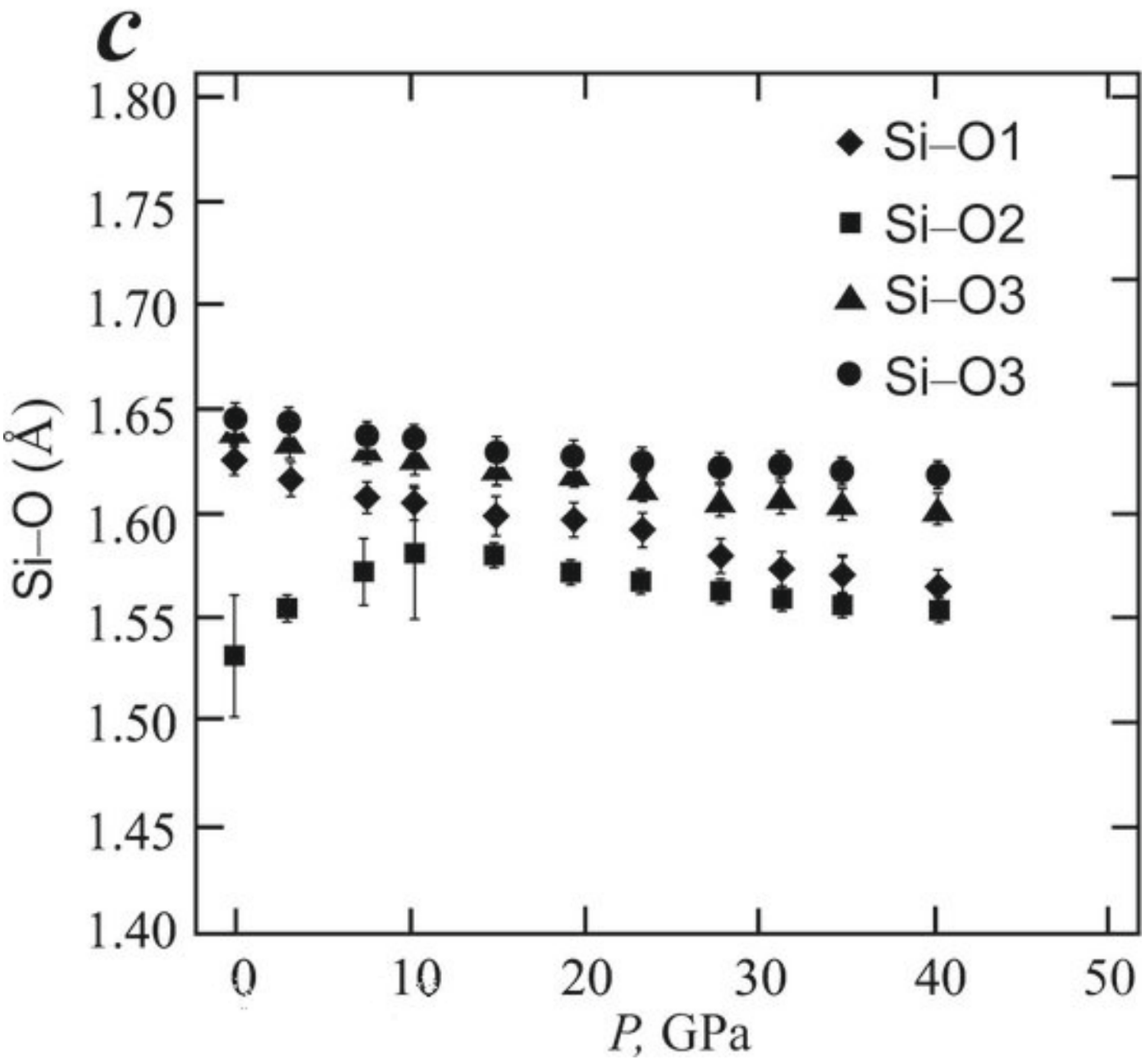
c
1.80
1.75
1.70
1.65
1.60
1.55
1.50
1.45
1.40
Si–O (Å)
Si–O1
Si–O2
Si–O3
Si–O3
0
10
20
30
40
50
P, GPa

Figure 7a

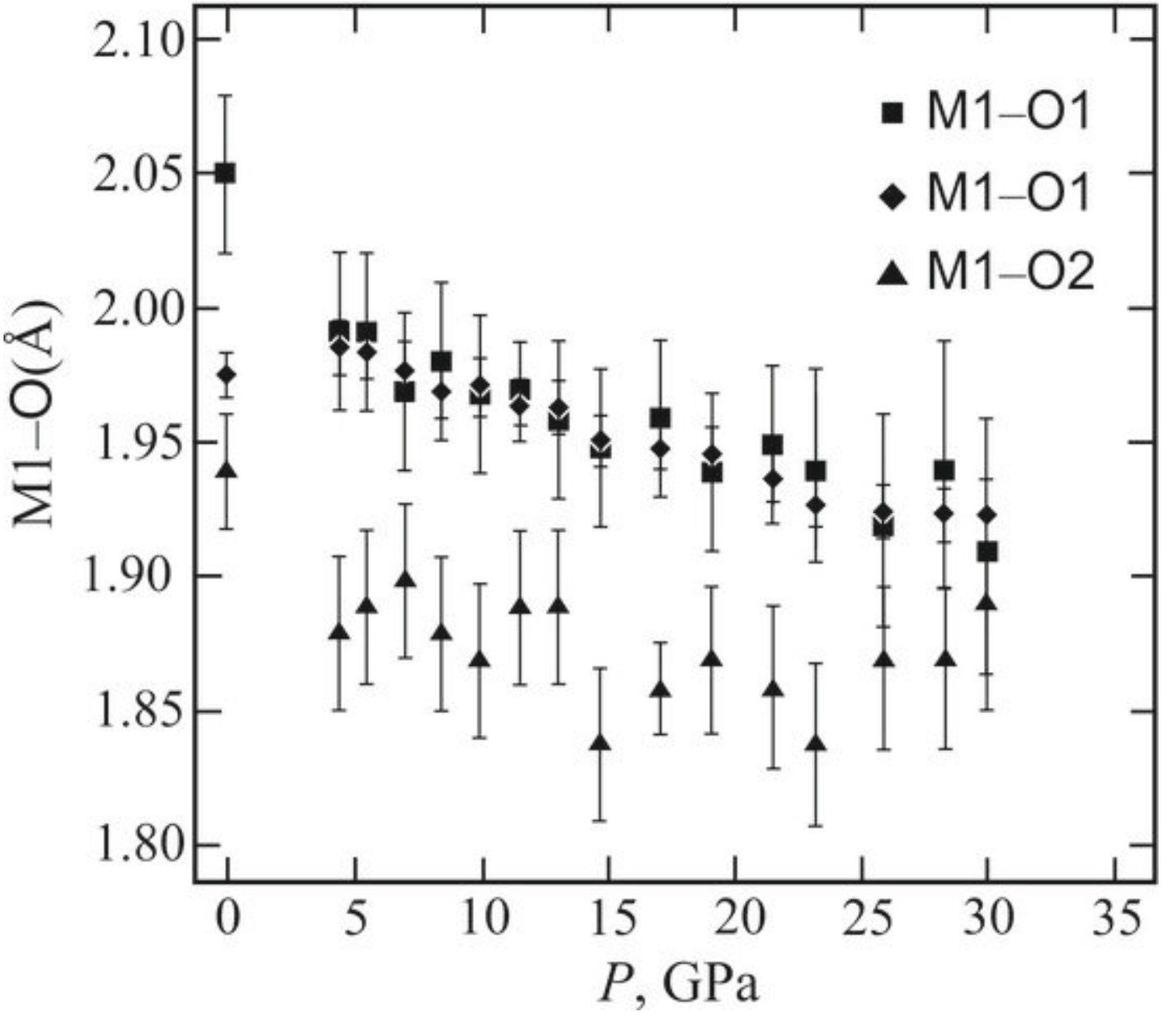
2.10
2.05
2.00
1.95
1.90
1.85
1.80
M1–O(Å)
0
5
10
15
20
25
30
35
P, GPa
M1–O1
M1–O1
M1–O2

Figure 7b

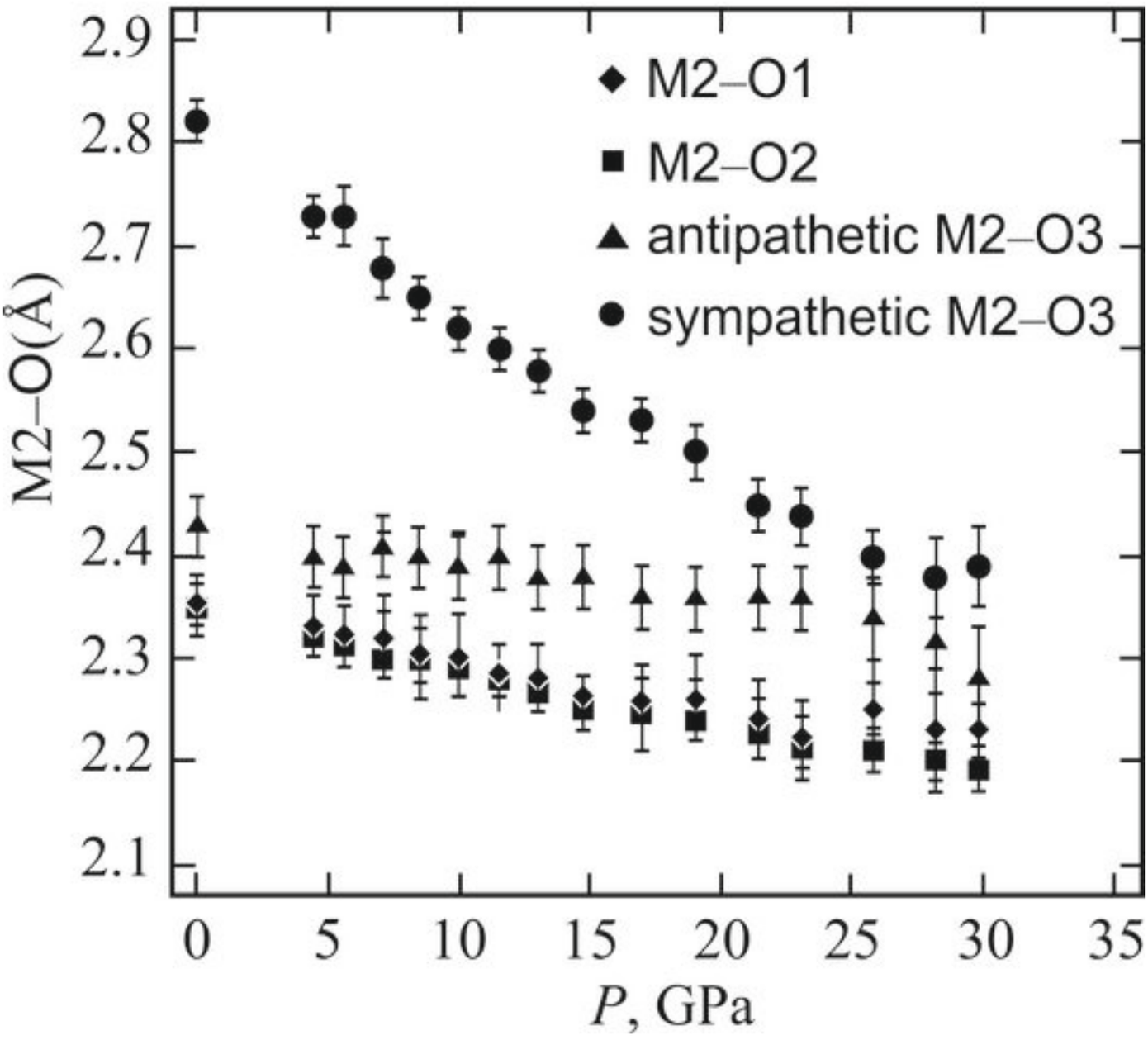
M2–O1
M2–O2
antipathetic M2–O3
sympathetic M2–O3
M2–O(Å)
2.9
2.8
2.7
2.6
2.5
2.4
2.3
2.2
2.1
0
5
10
15
20
25
30
35
P, GPa

Figure 7c

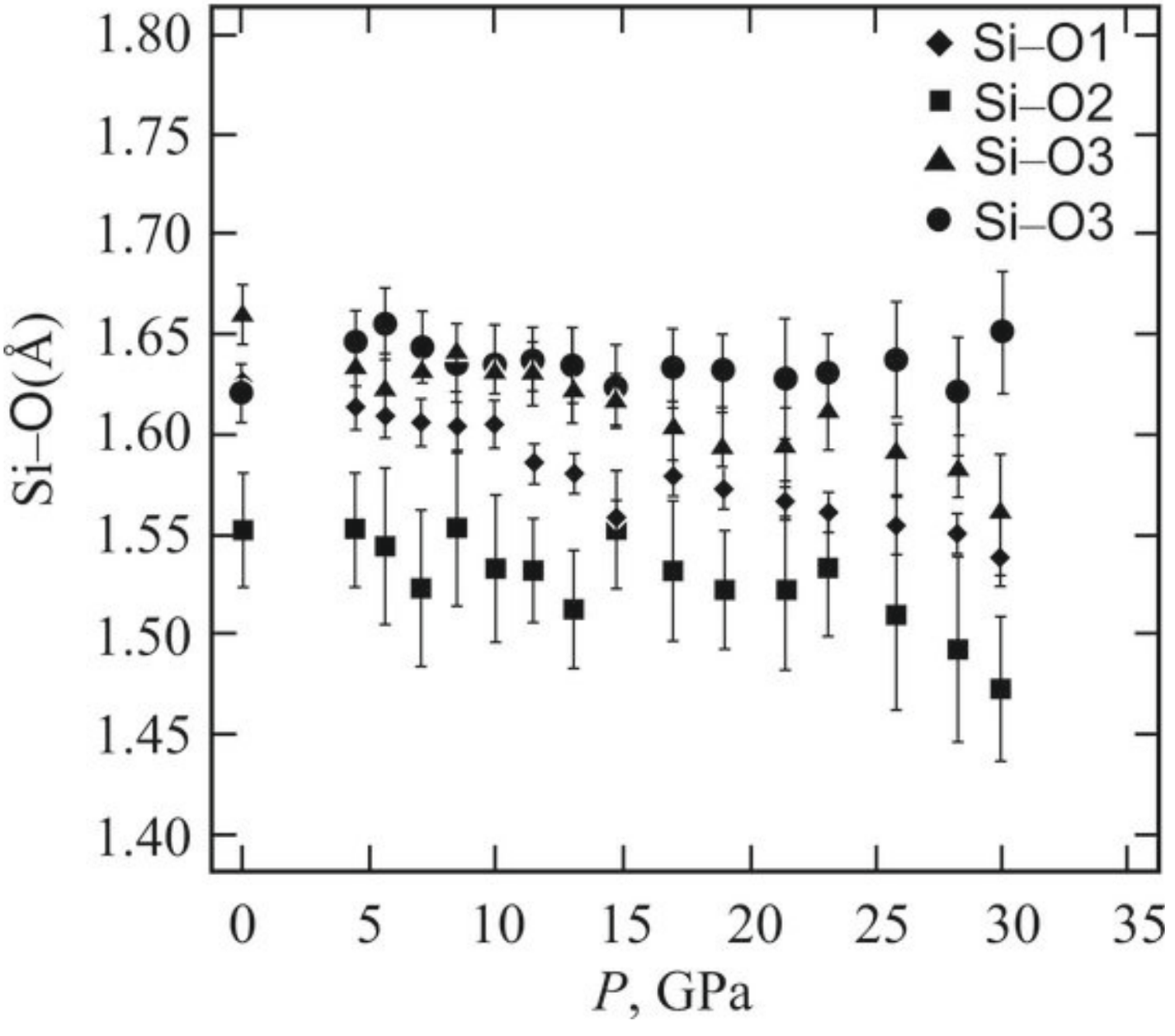
Si–O1
Si–O2
Si–O3
Si–O3
Si–O(Å)
1.80
1.75
1.70
1.65
1.60
1.55
1.50
1.45
1.40
0
5
10
15
20
25
30
35
P, GPa

Figure 8

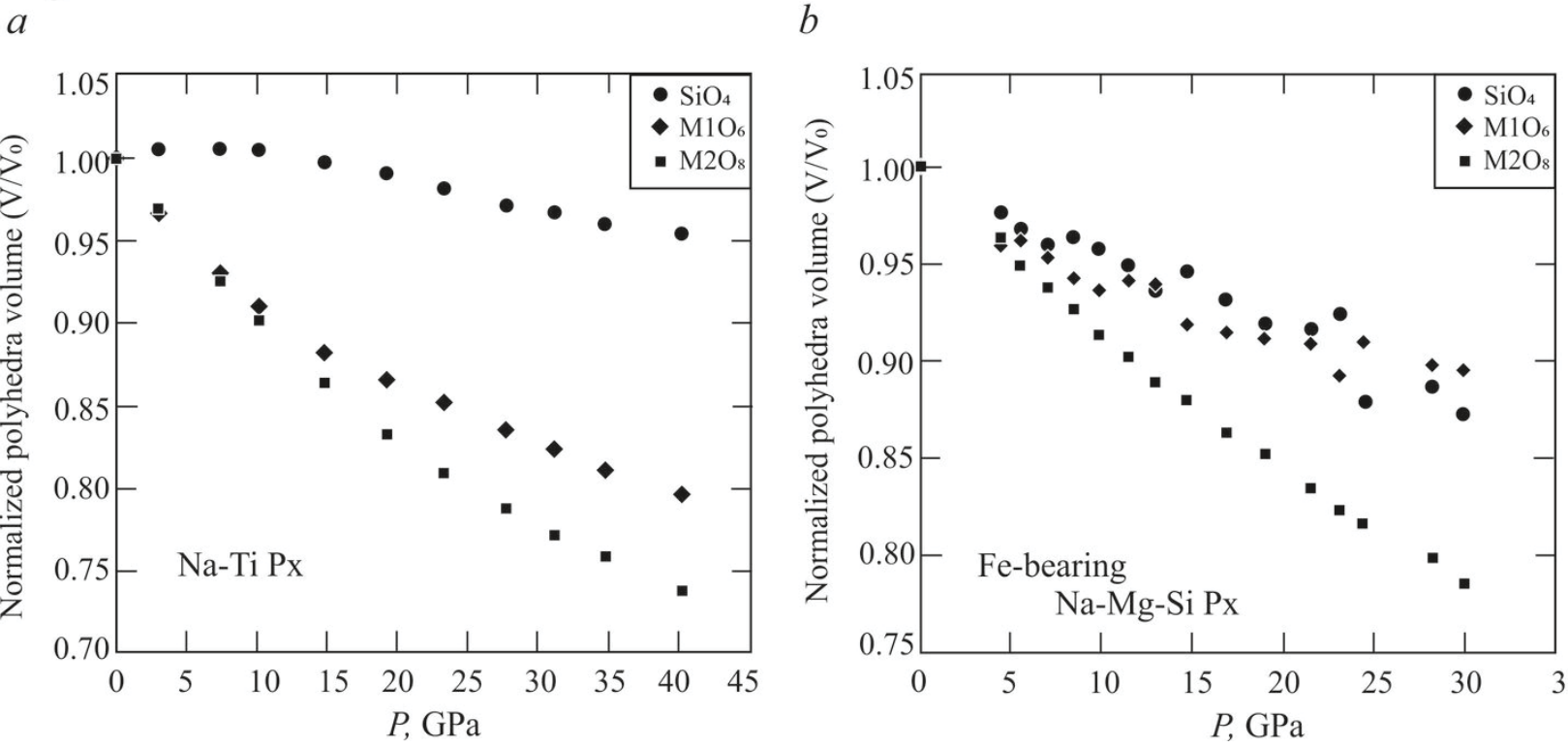
a
b
Normalized polyhedra volume (V/V0)
P, GPa
SiO4
M1O6
M2O8
Na-Ti Px
Fe-bearing
Na-Mg-Si Px

Figure 9

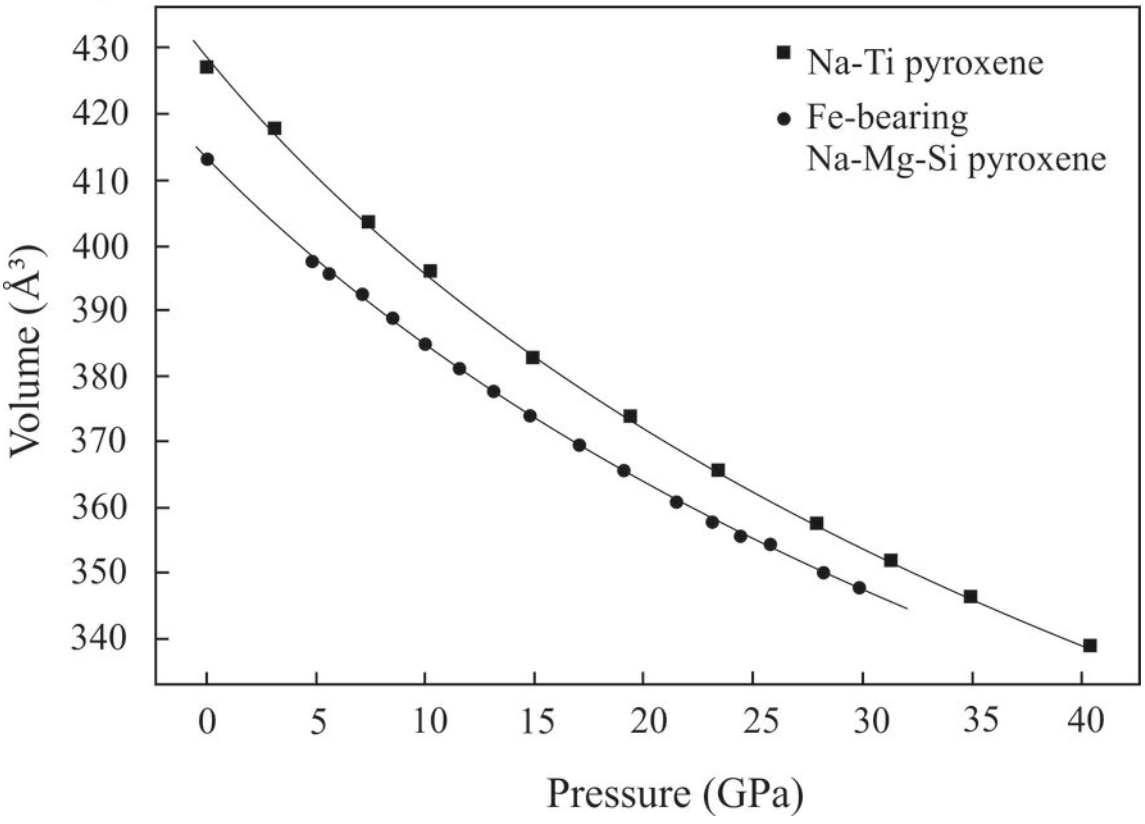
Na-Ti pyroxene
Fe-bearing
Na-Mg-Si pyroxene
Volume (Å³)
430
420
410
400
390
380
370
360
350
340
0
5
10
15
20
25
30
35
40
Pressure (GPa)

Figure 10

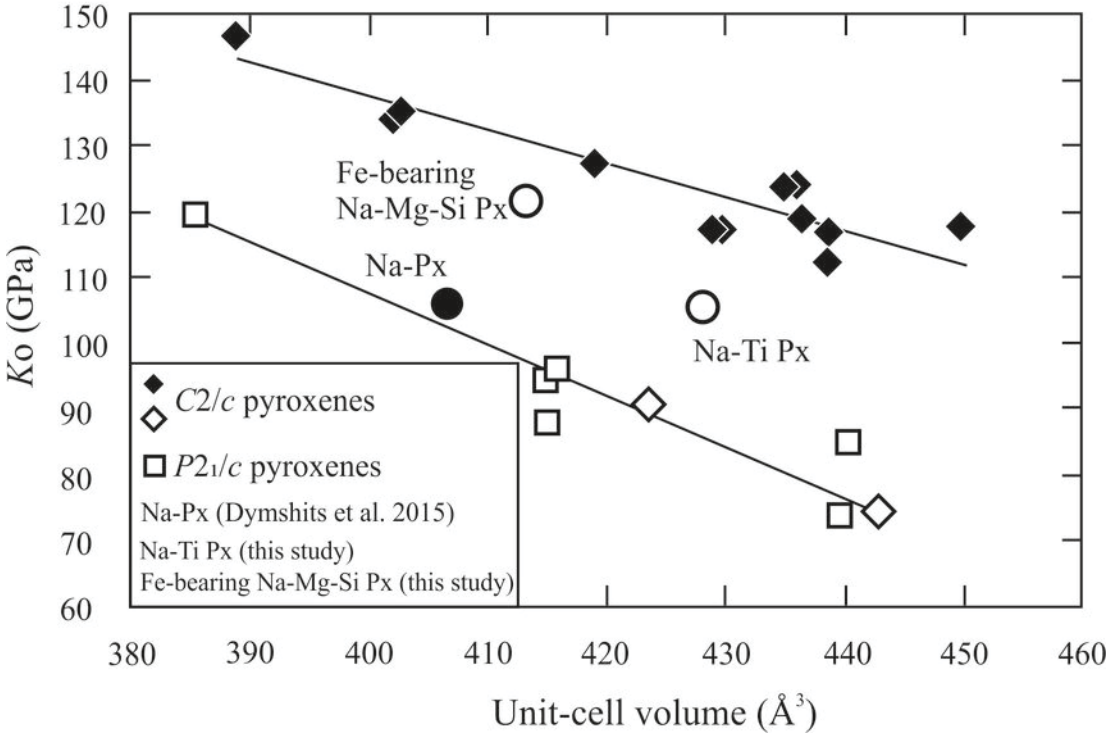
150
140
130
120
110
100
90
80
70
60
Ko (GPa)
380
390
400
410
420
430
440
450
460
Unit-cell volume (Å3)
Fe-bearing
Na-Mg-Si Px
Na-Px
Na-Ti Px
C2/c pyroxenes
P21/c pyroxenes
Na-Px (Dymshits et al. 2015)
Na-Ti Px (this study)
Fe-bearing Na-Mg-Si Px (this study)